Understanding the difference in fragility of the bcc phases of highly compressed P, As, and Sb through first-principles investigations

Masaaki Geshi [1], Hiroki Funashima,[2] and Gayan Prasad Hettiarachchi [1]

[1] *R^3 Institute for Newly-Emerging Science Design, Osaka University, 1-2 Machikaneyama, Toyonaka, Osaka 560-0043, Japan*

[2] *Department of Comprehensive Engineering, Kindai University Technical College, 7-1 Kasugaoka, Nabari, Mie 518-0459, Japan*

(Received 9 March 2023; revised 10 August 2023; accepted 29 August 2023; published 26 September 2023)

Among the pnictogens, the high-pressure phases of P show various structural transitions, while those of As and Sb do not. The body-centered-cubic (bcc) structure appears at 97 GPa in As and at 28.8 GPa in Sb. A transition from this strongly stable bcc structure to a new phase with further compression has not yet been reported in As or Sb in experimental or theoretical studies. The difference in the stability of the bcc structure between As (or Sb) and that of P is explained based on the investigations of the electronic structures using first-principles calculations. The occupied *d* orbitals of As and Sb play an important role in the stability of their respective bcc structures, while the absence of such in P causes an instability in the bcc structure making it comparatively fragile.

DOI: 10.1103/PhysRevB.108.094112

I. INTRODUCTION

In group V, P, As, Sb, and Bi are experimentally reported to have more or less a similar structural-transition sequence under high pressure. Among these elements, the high-pressure phase transitions of P have been investigated under much higher pressure both experimentally and theoretically [1–12]. The most stable structure of P at ambient conditions is the orthorhombic *A*17 structure (*Cmca*) [1,2]. This transforms into the rhombohedral $R\bar{3}m$ structure at 4.5 GPa and into the simple cubic (sc) structure ($Pm\bar{3}m$) at 10 GPa [3]. This phase is stable over a wide pressure range up to 107 GPa. The sc phase then transforms into the simple hexagonal (sh) structure (*P*6/*mmm*) at 137 GPa via an intermediate phase [4]. The structure of the intermediate phase was theoretically proposed by Ishikawa *et al.* using metadynamics simulations to be a modulated structure of the monoclinic lattice [5]. Fujihisa *et al.* reported that the structure of the intermediate phase is an incommensurately modulated structure based on experiments [6]. The detailed structure of the incommensurate phase was determined as *Cmmm* (00γ) *s*00 by Marqués *et al.* [7]. Next, the sh structure transforms into the body-centered-cubic (bcc) structure ($Im\bar{3}m$) at 262 GPa [8]. However, Sugimoto *et al.* showed that this phase is in fact a 2×2×2 superlattice of the bcc structure, namely, the *cI*16 structure based on experiments up to 340 GPa [9]. To date, there are no experimental works at higher pressure above this, except for computational ones. Mikhaylushkin *et al.* proposed that the bcc structure transforms to the hexagonal-close-packed (hcp) structure via an intermediate *IM*7 phase above 280 GPa [10]. The recent study by Flores-Livas *et al.* reported that the sh structure transforms into the bcc structure, next the bcc structure transforms into the *cI*16 structure, and finally the *cI*16 structure transforms into the hcp structure [11]. Zhuang *et al.* investigated the higher-pressure region up to 2 TPa and reported that the hcp structure transforms into the face-centered-cubic (fcc) structure at 1.35 TPa [12].

In the face of the rich variety of high-pressure phases exhibited by P, As and Sb are comparatively very simple. The ground state of As at ambient conditions takes the *A*7 structure. The *A*7 structure then transforms into the sc structure at 25 GPa [13]. The sc structure transforms into an intermediate phase at 48 GPa, and finally transforms into the bcc structure at 97 GPa [14]. The structure of the intermediate phase was identified to be a body-centered host-guest (HG) structure by Degtyareva *et al.* [15]. A recent experimental study by Akahama *et al.* reported that the transition from the sc to HG structure occurs at around 52 GPa, the transition from the HG to bcc structure occurs at around 126 GPa, and the bcc structure remains stable at least up to 250 GPa [16]. The bcc structure remains strongly stable with no potential high-pressure phases theoretically as well.

Following the footsteps of As, Sb also exhibits a similar structural sequence under compression. The *A*7 structure transforms into a HG structure at 8 GPa, and the HG structure then transforms into the bcc one at 28 GPa [17]. Degtyareva *et al.* found an incommensurate to incommensurate transition in the range less than 10 GPa [16]. The bcc structure is stable up to 65 GPa, with no further experiments exploring much high-pressure region thus far. Recently, Geshi *et al.* reported that the bcc structure of Sb is stable at least up to 1000 GPa from a first-principles-based comprehensive structure search [18]. Moreover, the phonon band dispersions and the electronic density of states (DOS) pointed to the remarkable stability of the bcc structure. As discussed later, As also shows quite similar trends closely following the example of Sb.

In many cases, the sequences of high-pressure phases of elements within the same group follow similar footprints. This is primarily attributed to the fact that the elements of the same family have the same valence electrons, and this tendency is stronger at higher pressures. Among them, the elements in periods 4 and 5 tend to be similar. Period 3 is different because of the absence of 2*d* orbitals, and there is a difference between periods 2 and 1 because of the absence of 1*p* orbitals.

Another noteworthy feature is that similar high-pressure phases appearing in the sequence are realized on the low-pressure side in the heavier elements within the group. In the case of chalcogen, a β-Po type rhombohedral structure appears in the high-pressure phases of S, Se, and Te. This phase of S appears at 162 GPa [19], that of Se does at 60 GPa [20], and that of Te does at 11 GPa [21]. The next high-pressure phase, which is the bcc structure, appears at 140 GPa for Se [20] and at 27 GPa for Te [22]. For S, on the other hand, the next high-pressure phase is yet to be observed in experiments. The next predicted phase in theory is an incommensurate HG structure followed by the bcc structure at 679 GPa from first-principles calculations with the PBE96 functional [23]. The experimentally observed next high-pressure phase of Te after the bcc structure is the face-centered-cubic (fcc) one, which coexists with a double hcp (dhcp) one from 100 to 160 GPa. Above 160 GPa, the dhcp structure disappears and the fcc structure remains intact [24,25]. These detailed behaviors were also confirmed from reliable first-principles calculations by Geshi *et al.* [26]. Reasoning based on the case of Te, the next high-pressure phase of Se and S is likely the fcc structure. However, this has not been reported experimentally, nor theoretically.

In this work, we particularly focus on the pnictogens P, As, and Sb. As described earlier, the sequences of high-pressure phases are similar between As and Sb. While various high-pressure phases have been found experimentally and also predicted theoretically for P, no candidate high-pressure phases for As and Sb following the bcc one has been reported. This is in stark contrast to the chalcogens where similar high-pressure phases appearing in the sequence are realized on the low-pressure side in the heavier elements within the group. An important question is whether any of the structures appearing in compressed P could possibly appear in Sb or As after the seemingly robust bcc phase. To investigate this possibility, we performed an extensive structural search based on first-principles calculations [17]. Based on the obtained crystal structures and phonon dispersion profiles, we report herein the instability of the bcc structure of P observed within a comparatively very narrow pressure region, and that the bcc structure of As in contrast is strongly stable up to around 2200 GPa over a wide pressure region and transitions to the hcp structure at higher pressures. Before reluctantly transitioning to the hcp structure, the bcc structure of As remains strongly stable over a wide pressure range quite similar to that of Sb. The next important question is why does As and Sb demonstrate such robustly stable bcc phases over a wide pressure range, while that of P is found in a very narrow pressure range and is comparatively unstable? In order to answer this, we investigated the electronic structures of the bcc phases found in P, As, and Sb. Based on the obtained results we discuss the potential origin behind this atypical behavior.

II. COMPUTATIONAL DETAILS

We performed first-principles electronic structure calculations based on the density functional theory (DFT) to determine the crystal and electronic structures. We used the QUANTUM-ESPRESSO package [27] to perform total energy calculations, structural relaxations, and phonon calculations with the Perdew-Burke-Ernzerhof (PBE)–type generalized gradient approximation (GGA) [28] as an exchange-correlation functional and ultrasoft pseudopotentials (USPP) [29]. The valence electron configurations of P, As, and Sb are five electrons consisting of $3s^2\,3p^3$, $4s^2\,4p^3$, and $5s^2\,5p^3$, respectively. The validity of this USPP is discussed in detail in the Supplemental Material [30]. The cutoff radius of the local potential was set to 1.8, 2.0, and 2.1 a.u. for P, As, and Sb, respectively. The cutoff energy of the wave function $E_{\rm cut}$ was 80 Ry for P and Sb, and 60 Ry for As. The cutoff energy for the charge density was set 12 times the $E_{\rm cut}$. The Brillouin zone for each structure containing four atoms was sampled using Monkhorst-Pack k-point meshes of $24\times24\times24$ for P and Sb, and $32\times32\times32$ for As. In determining these values, test calculations were performed to ensure that the total energy precision was sufficient to estimate the difference in energy and enthalpy between the relaxed structures. The errors were found to be up to 2 meV/atom, and in many cases smaller. Occasionally, $E_{\rm cut} = 120$Ry was used for validation purposes, but there were no essential differences in the results. Ensuring the computational precision with the aforementioned parameters, we performed an extensive structure search using an original method developed by us [26,31]. Initial structures from the space group index 75 (*P4*) to 230 ($Ia\bar{3}d$) were generated for a unit cell consisting of four atoms. These covered the tetragonal, trigonal, hexagonal, and cubic structures as initial structures. The subsequent structural relaxations were performed assuming only the Bravais lattice. In addition, we performed a structure search in a random manner at given pressure values. We did not perform the structural relaxation for all the randomly generated initial structures. Instead, we picked a set of low enthalpy structures obtained from a self-consistent field calculation and performed a full optimization on those chosen ones only. We generated 200 initial structures and selected 20 low enthalpy structures for further investigations.

We performed all-electron electronic structure calculations using the full-potential linearized augmented plane wave (FLAPW) method [32] to confirm the precision of the pseudopotential. The $R_{\rm MT}K_{\rm max}$ was set to 10, and the k-point sampling was set to 110 or 165 points in the irreducible Brillouin zone. The PBE-type GGA [28] was used in all the calculations.

III. RESULTS AND DISCUSSION

A. Instability of the bcc structure of P

The enthalpies of the bcc, sh, hcp, dhcp, fcc, *Cmcm*, and *cI*16 structures of P are shown with respect to the enthalpy of the bcc structure from 190 to 510 GPa in Fig. 1(a). Figure 1(b) provides an enlarged view of the same at the vicinity of the transitions from the bcc to c*I*16 and from c*I*16 to hcp structures. These structures have four atoms per unit cell. All plotted data except for *cI*16 are obtained from the structure search and were not assumed. Only the enthalpy of the *cI*16 structure was calculated with an assumed cell containing one atom with crystal symmetry. Up to 220 GPa, the lowest enthalpy structure is the sh structure, and the second lowest is

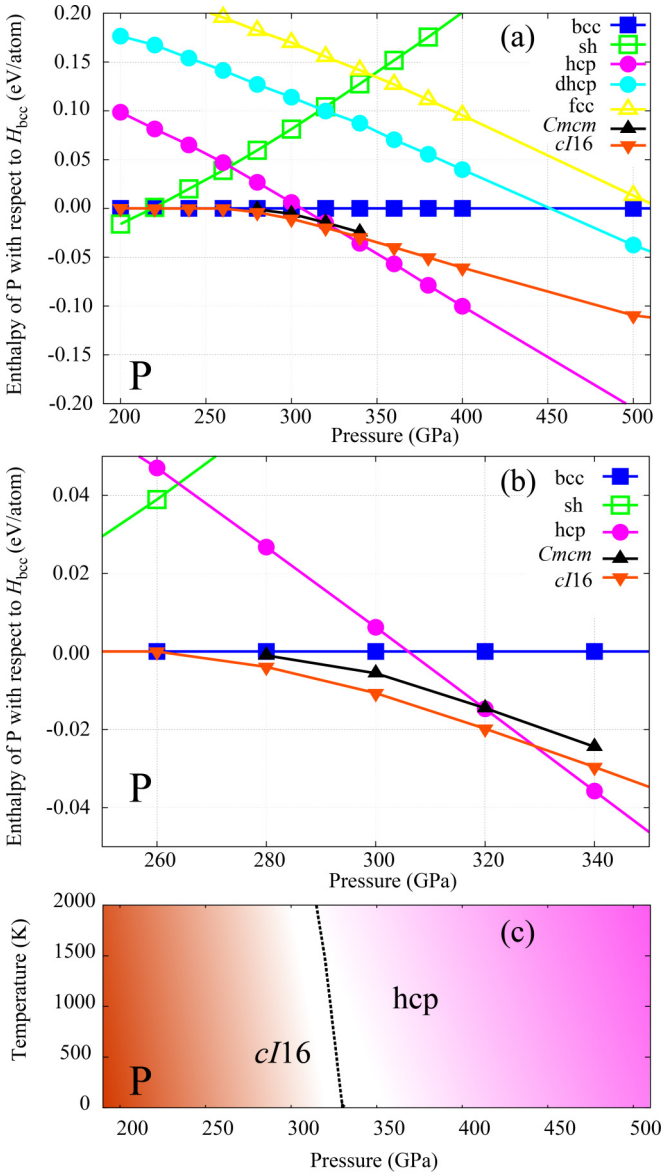

FIG. 1. (a) The calculated enthalpies H of various crystal structures of P with respect to the enthalpy of the bcc structure as a function of pressure in the pressure range 190–510 GPa. (b) Enlarged version of the calculated enthalpies H of various crystal structures of P with respect to the enthalpy of the bcc structure as a function of pressure in the pressure range 250–350 GPa, which contains transitions from bcc to $cI16$ and from $cI16$ to hcp. The solid lines are guides to the eye. (c) The pressure-temperature phase diagram of P. The dotted line denotes the boundary between the $cI16$ and hcp structures.

the bcc one. The $cI16$ structure [$I\bar{4}3d$, 16c (x, x, x)] is closely related to the bcc structure. When x is zero, the $cI16$ structure becomes bcc. The structural relaxations of the $cI16$ structures were performed over a pressure range 200–500 GPa, using nonzero parameters of x as initial values. As a result, the structures in the range 200–260 GPa converged to the bcc one with $x = 0$, and the others converged to $cI16$ with nonzero values. The obtained x values at 280, 300, and 320 GPa are 0.0198, 0.0249, and 0.0259, respectively. These are consistent with

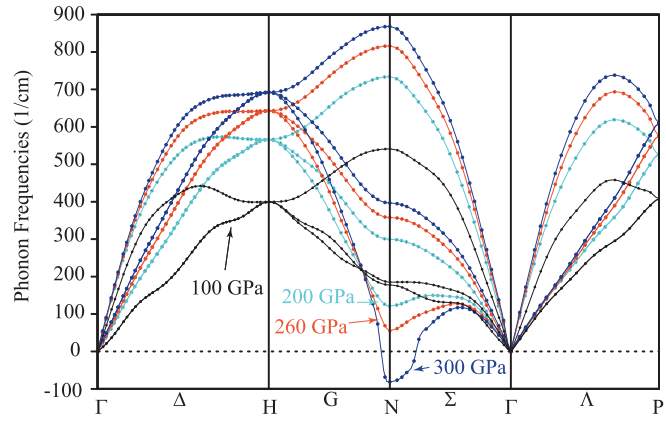

FIG. 2. The phonon dispersion curves of bcc P at 100, 200, 260, and 300 GPa. The solid lines are guides to the eye.

the experimentally obtained value of 0.0244(3) [9]. Above 320 GPa, the hcp structure is the lowest enthalpy structure up to 1000 GPa according to our calculations.

The bcc structure can be considered as a special case of the *Cmcm* structure [4c $(-y, y, 1/4)$, $(y, -y, -1/4)$]. If $a = a_{bcc}$, $b = \sqrt{2}b_{bcc}$, $c = \sqrt{2}c_{bcc}$, and $y = 1/4$, then C_4, C_3, and C_2' symmetries are ensured. As a result, the *Cmcm* structure is equivalent to the bcc structure. The hcp structure can be also considered as a special case of the *Cmcm* structure. If $a = a_{hcp}$, $b = \sqrt{3}b_{hcp}$, $c = c_{hcp}$, and $y = 1/6$, then C_6 and C_2' symmetries are ensured. As a result, the *Cmcm* structure is equivalent to the hcp structure. Here, a_{bcc}, b_{bcc}, and c_{bcc} are the lattice constants of the bcc structure, and a_{hcp}, b_{hcp}, and c_{hcp} are the lattice constants of the hcp structure. The *Cmcm* structure is the lowest enthalpy structure in the pressure range from 280 to less than 320 GPa for a unit cell consisting of four atoms. The $cI16$ structure consists of unit cells with 16 atoms. Therefore, the *Cmcm* structure can be considered as the resultant structure when the unit cell is restricted to four atoms.

Figure 1(c) shows the pressure-temperature phase diagram calculated by using PHONOPY within a quasiharmonic approximation (QHA) [33]. The Gibbs' free energies of the bcc, hcp, dhcp, fcc, sh, and $cI16$ structures were compared and the structure with the lowest free energy is shown at each pressure of every 10 GPa near the boundary, and of 20–50 GPa otherwise. It is noted that the QHA is not a good approximation for noncubic crystals since it assumes an isotropic continuum model.

The phonon dispersion curves pertaining to the bcc structure of compressed P are shown in Fig. 2. The phonons in the Σ direction begin to soften below 200 GPa and demonstrate imaginary frequency values between 260 and 300 GPa. According to the enthalpy, the bcc structure is stable from 220 to 260 GPa as shown in Fig. 1. As we can observe in Fig. 1, the sh phase has the lowest enthalpy below 220 GPa, around which the bcc phase becomes more stable. It is noted that the enthalpy of the bcc phase is the same as that of $cI16$, which is the same structure when $x = 0$. However, above 260 GPa, the $cI16$ structure becomes more stable than bcc, as x assumes values greater than 0. The phonon profiles indicate that the bcc structure is becoming unstable starting at pressures con-

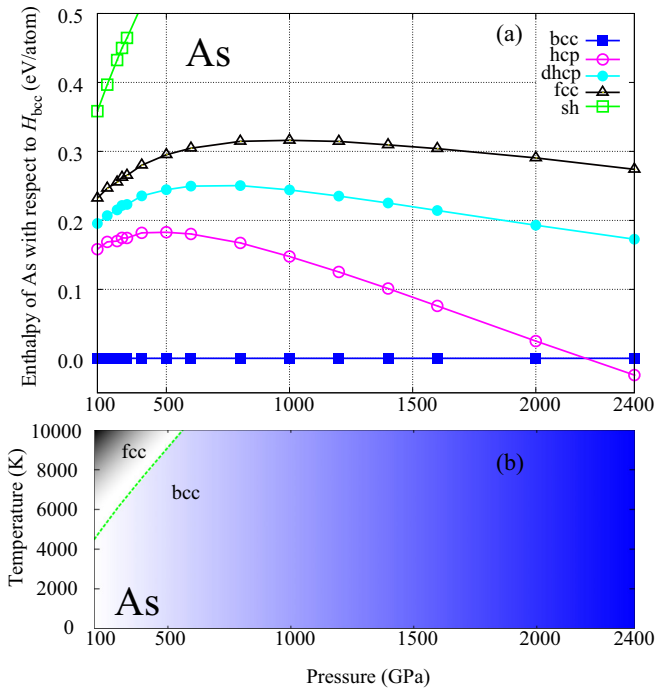

FIG. 3. (a) The calculated enthalpies H of As with respect to the enthalpy of the bcc structure as a function of pressure from 100 to 2400 GPa. The solid lines are guides to the eye. (b) The pressure-temperature phase diagram of As. The dotted line denotes the phase boundary between the bcc and fcc structures.

siderably lower than 220 GPa. The origin and onset of this instability are discussed from the perspective of the electronic structure later.

B. Stability of the bcc structure of As

Figure 3 shows the enthalpies of the hcp, dhcp, fcc, and sh structures of compressed As with respect to that of the bcc structure as a function of pressure from 100 to 2400 GPa. The lowest enthalpy structure is the bcc one below about 2200 GPa. Above 2200 GPa, the hcp structure becomes the lowest enthalpy structure.

The transition pressure from the bcc to hcp structure depends on the USPP. When the USPP treats the 3d electrons as valence electrons in a 15-electron $3d^{10}\,4s^2\,4p^3$ USPP, the transition point shifts to higher pressure. This is because the orthogonality of the 3d and 4d electrons makes it difficult for 4d electrons to exist near the Fermi level when the 3d electrons are treated as valence electrons, and as a result the bcc structure remains intact up to higher pressure. On the other hand, if the 3d electrons are treated as core electrons, the 4d electrons tend to appear near the Fermi level and the bcc structure becomes unstable at lower pressures. However, in actual calculations, the effect of the orthogonality is negligible up to around 2000 GPa [29]. An accurate estimate of the transition pressure needs to be investigated by fundamentally reviewing the pseudopotential based on its accuracy.

Tsuppayakorn-Aek *et al.* performed a structure search for high pressure As, and reported a body-centered-tetragonal (bct) structure with the space group $I4_1/acd$ [34] after the

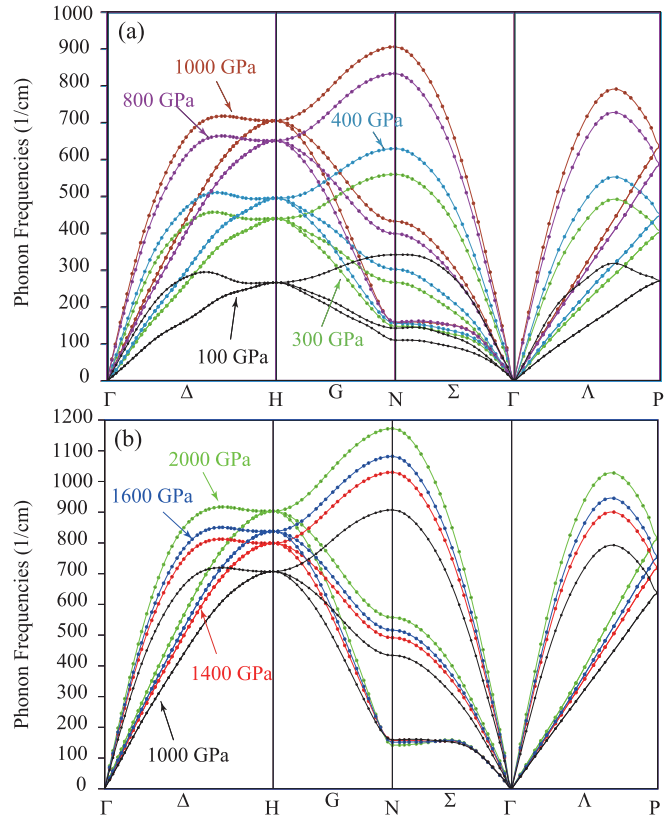

FIG. 4. The phonon dispersion curves of bcc As (a) at 100, 300, 400, 800, and 1000 GPa and (b) at 1000, 1400, 1600, and 2000 GPa. The solid lines are guides to the eye. The phonon band dispersion at 1000 GPa is shown in both panels for easy comparison.

HG structure instead of a bcc one. A similar structure was observed in our structure search as well, however, the enthalpy was much higher than the bcc structure. Tsuppayakorn-Aek *et al.* used a cutoff energy of 280 eV (=20.58 Ry) in their structure search. The authors also mentioned that the enthalpy difference between the bcc and bct structures was 1 meV/atom. Due to the low cutoff energy used in their calculations, such an enthalpy difference cannot be discussed precisely. We optimized their proposed bct structure as an initial structure with a cutoff energy of 80 Ry under both types of USPP (that is, 3d electrons treated as either core or valence) in the pressure range 100–300 GPa, and the stable structure becomes the bcc one in either case. In addition, in our calculations, the error in the computational precision when the pseudopotential treats the 3d electrons as valence is ten times more than when the pseudopotential treats the 3d electrons as core electrons. For these reasons, the bct structure was eliminated from further consideration.

Figure 3(b) shows pressure-temperature phase diagram calculated within the QHA. The Gibbs' free energies of the bcc, hcp, dhcp, and fcc structures were compared and the structure with the lowest free energy is shown at each pressure of every 10–20 GPa near the boundary of the transition from bcc to hcp, and of 100 GPa otherwise.

In comparing As with Sb, the lowest enthalpy structure for Sb is the bcc one even at 2000 GPa, the highest pressure of the calculations. The second, third, and fourth lowest enthalpy

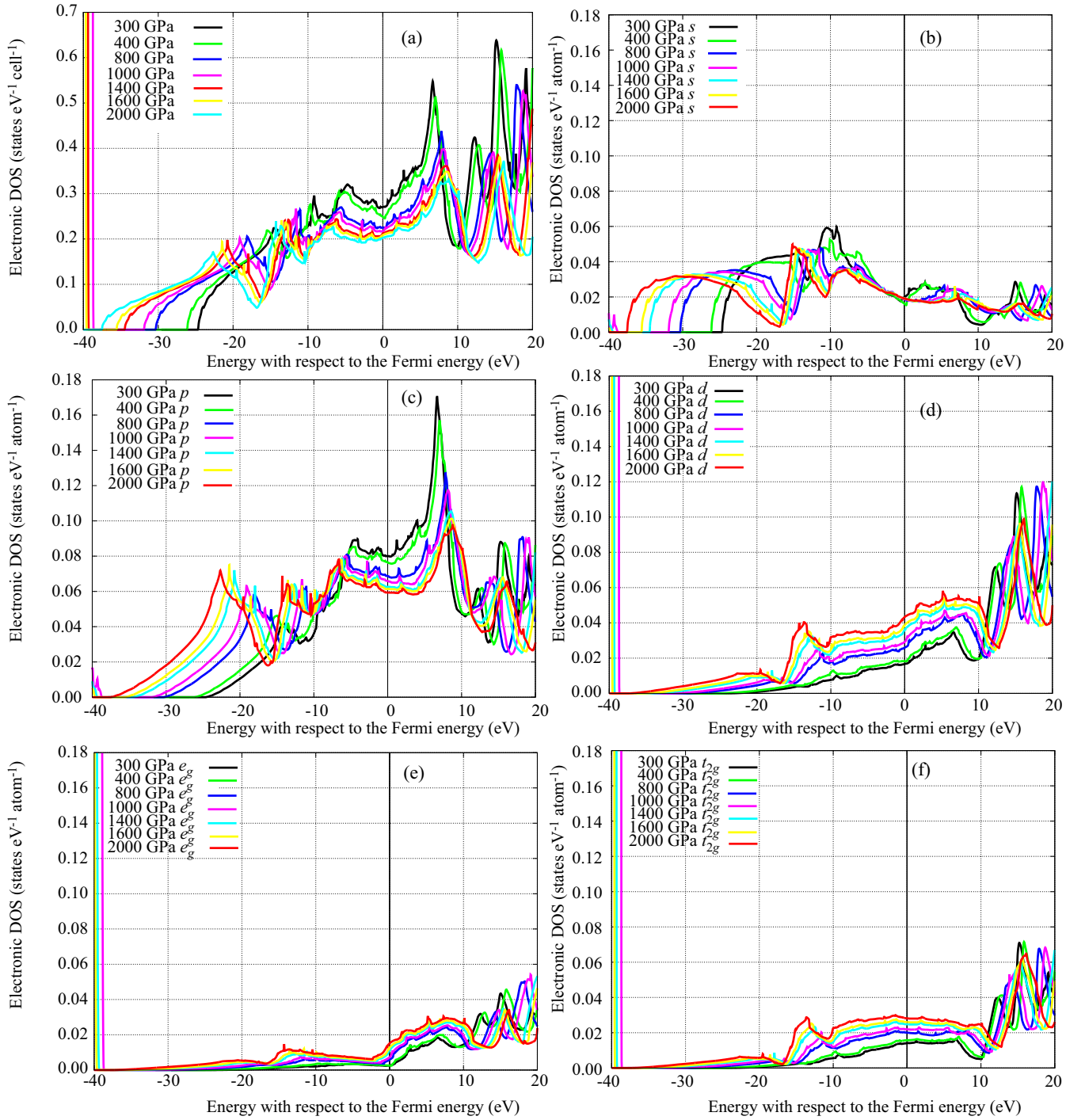

FIG. 5. The evolution of the DOS of compressed As in the strongly stable bcc phase at 300, 400, 800, 1000, 1400, 1600, and 2000 GPa with the same MT sphere of 1.77 bohrs. Panels show the pressure dependence of the (a) total DOS, (b) *s* states, (c) *p* states, (d) *d* states, (e) e_g states, and (f) t_{2g} states.

structures are the dhcp, hcp, and fcc structures, respectively as reported earlier for Sb [17]. This order changes around 1200 GPa, and the second one becomes the hcp structure and the third one becomes the dhcp structure. However, the enthalpy difference between the bcc structure and other three structures is still widening even at 2000 GPa with no indication of a transition from bcc to another. In comparing As with P, a recent study predicted that the hcp structure of P transforms to the fcc structure at 1350 GPa [12]. However, even if the fcc structure becomes the lowest enthalpy structure for As after the hcp structure in following the footsteps of P, the pressure is much higher as inferred from Fig. 3.

Figure 4 shows the phonon dispersion curves of As in the bcc phase from 100 to 1000 GPa and from 1000 to 2000 GPa in panels (a) and (b), respectively. The phonon profiles indicate that the bcc structure of compressed As is very stable in a very wide pressure range, in contrast to P. We note that the phonon profiles at the *N* point in the Σ direction may be

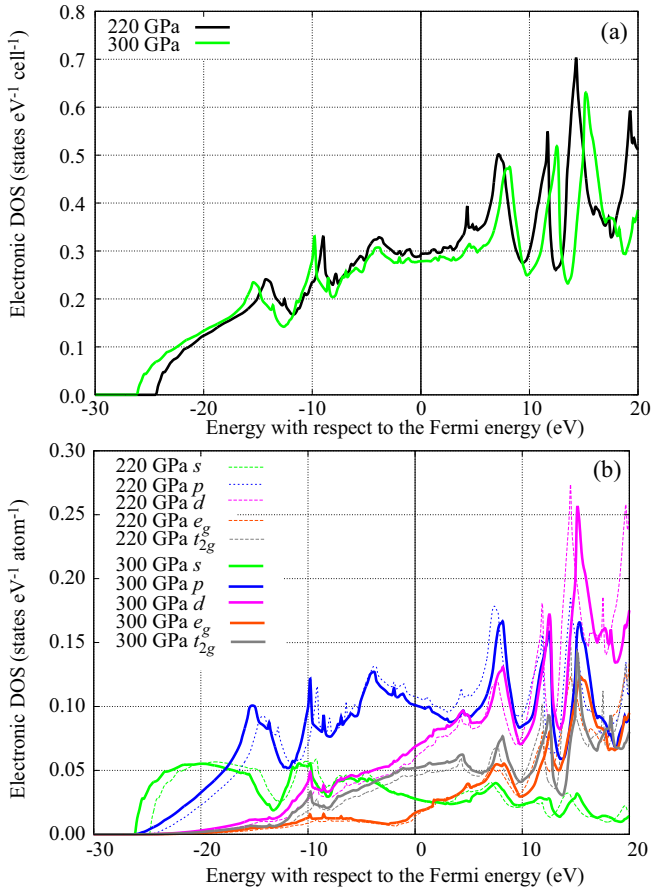

FIG. 6. The DOS of compressed P in the bcc phase at 220 and 300 GPa calculated with the same MT sphere of 1.96 bohrs. Panels (a) and (b) show the total DOS and the partial DOS, respectively.

hinting to an onset of instability of the bcc structure above 1000 GPa. However, the bcc structure by far has the lowest enthalpy as seen in Fig. 3. We also note that this behavior is quite similar to that of Sb [17]. In light of these results, it is evident that there are notable differences between compressed P and As (Sb) with respect to the structural phases, their stability, and the pressure range of stability, which could be stemming from underlying differences in the respective electronic structures of pnictogens under high pressure.

C. Electronic densities of states of As and P and their interpretation

In order to elucidate the origin of the strongly stable bcc phase of compressed As, the DOS were calculated as a function of pressure. Figures 5(a)–5(f) show the total DOS, s states, p states, d states, and d orbitals divided into e_g and t_{2g} states, respectively. The DOSs shown in Fig. 5 are calculated using a same muffin tin (MT) sphere of 1.77 bohrs, and the number of electrons in the MT sphere can be compared at different pressure values. The increase or decrease in DOS represents the increase or decrease in electrons within the MT sphere. Although more electrons are pushed into the MT sphere as the pressure increases, the orbital angular momentum ratio does not change. It is particularly important to note the increase or decrease in the states near the Fermi level,

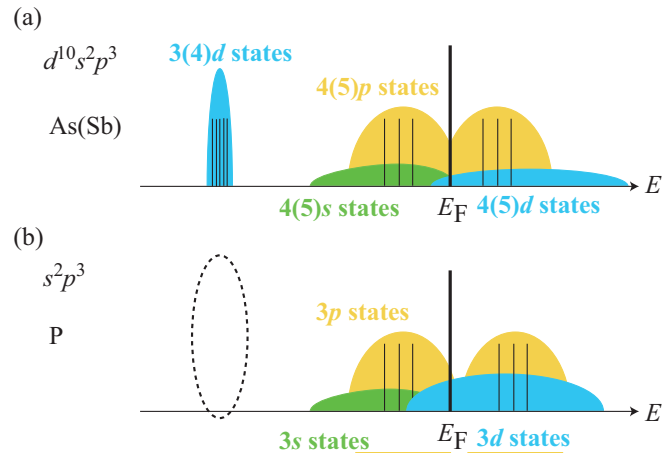

FIG. 7. The schematic view of the PDOS of (a) As (or Sb) and (b) P.

which are related to coupling. As can be seen from Fig. 5(a), the DOSs near the Fermi level do not change drastically with increasing pressure. Moreover, the s states at the Fermi level do not increase with increasing pressure as seen from Fig. 5(b). This means that the bonding and antibonding states are almost completely constructed by the p states shown in Fig. 5(c). There are notable changes, in which the p states at the Fermi level decrease and the d states [Fig. 5(d)] increase with pressure. The completely occupied 3d states lie below about -40 eV, and the partially occupied d states near the Fermi level are the 4d states. With increasing pressure, the increase in the t_{2g} states is greater than that of the e_g states among the d orbitals [Figs. 5(e) and 5(f)]. The aforementioned trends of As are quite similar to those of Sb [17].

Figures 6(a) and 6(b), respectively show the total and partial DOS (PDOS) of compressed P at 220 and 300 GPa calculated with a fixed MT sphere of 1.96 bohrs. The shape of the PDOSs of P near the Fermi level are different from those of As. The dip near the Fermi level in the total DOS of P is mainly constructed by the PDOS of the p states and PDOS of the d states as revealed by Fig. 6(b), while the dip in As is mainly constructed by the PDOS of the p states as revealed by Figs. 5(b)–5(d). From Fig. 6(b), the differences between the PDOS shown by the solid lines and those with the dotted lines indicate a transfer of the electronic states. At the vicinity of the Fermi level, the PDOSs of the s states do not change, while the PDOSs of the p and d states change, and the degree of change is almost identical. The increase in the PDOSs with increasing pressure is normal because these are calculated with a fixed MT radius. This change in the PDOSs implies that increasing pressure causes a transfer from the p state to the d state of the electronic state. Moreover, the transfer is mostly to the t_{2g} states. These d states near the Fermi level are the 3d states. Note that there are no occupied 3d states in P.

The aforementioned DOS results are illustrated in the schematic view shown in Fig. 7. The remarkable difference in the stability of the bcc structures of P and As (Sb) is fundamentally coupled to the differences in their respective electronic structures. The calculated electronic states can be interpreted as the formation of the bonding-antibonding state

composed of the p orbitals centered at the Fermi level. Because of the presence of the fully occupied d orbitals in As (Sb), there is no room for many unoccupied d states near the Fermi level due to the orthogonality of the wave function. As a result, the bonding-antibonding state consists almost entirely of the p states, making it the most robust bonds possible. On the other hand, since there are no fully occupied d orbitals below the Fermi level in P, the d state appears near the Fermi level and the bonding-antibonding state composed only of the p orbital is disturbed. As a result, the bcc structure of P becomes unstable with pressure, and appears only in a narrow pressure range in the calculations compared to As (Sb).

The main reason for the difference between P and As (Sb) is that the $3d$ states of As ($4d$ states of Sb) are completely filled, whereas there are no occupied d states in P. The occupied d orbitals play an important role in preventing the deformation of the crystal structure in space, which is also related to the orthogonality of the wave function. For this reason, P without occupied d orbitals cannot realize a stable bcc structure because there is no reinforcement from an electronic point of view to prevent a spatial crystal-structure deformation. Therefore, the stable pressure region of the bcc phase becomes very narrow even in calculations, and may not be fully observed in experiments. On the other hand, As and Sb with their occupied d orbitals can strongly withstand high compression and retain the bcc phase without long-range deformations.

IV. CONCLUSONS

The high-pressure phases of P, As, and Sb were investigated using first-principles calculations, in particular to elucidate the differences among the strongly stable bcc structures of As and Sb and the fragile one of P, and understand the origin. The bcc structures of As and Sb under high pressure is very stable even above 1000 GPa because of the occupied d states. The presence of the occupied d orbitals is a major contributor to maintaining the stability of the bcc structure at high pressure. In the absence of this stabilizing factor in P, the bcc structure immediately becomes unstable and undergoes a variety of structural changes with increasing pressure. Here, we have provided a very clear explanation of these phenomena by analyzing the electronic profiles of each bcc structure.

ACKNOWLEDGMENT

This work was supported by JSPS KAKENHI, Grants-in-Aid for Scientific Research (C) (Grant No. 19K03717).

[1] R. Hultgren, N. S. Gingrich, and B. E. Warren, The atomic distribution in red and black phosphorus and the crystal structure of black phosphorus, J. Chem. Phys. **3**, 351 (2004).
[2] A. Brown and S. Rundqvist, Refinement of the crystal structure of black phosphorus, Acta Cryst. B **19**, 684 (1965).
[3] T. Kikegawa and H. Iwasaki, An x-ray diffraction study of lattice compression and phase transition of crystalline phosphorus, Acta Cryst. B **39**, 158 (1983).
[4] Y. Akahama, M. Kobayashi, and H. Kawamura, Simple-cubic–simple-hexagonal transition in phosphorus under pressure, Phys. Rev. B **59**, 8520 (1999).
[5] T. Ishikawa, H. Nagara, K. Kusakabe, and N. Suzuki, Determining the Structure of Phosphorus in Phase IV, Phys. Rev. Lett. **96**, 095502 (2006).
[6] H. Fujihisa, Y. Akahama, H. Kawamura, Y. Ohishi, Y. Gotoh, H. Yamawaki, M. Sakashita, S. Takeya, and K. Honda, Incommensurate Structure of Phosphorus Phase IV, Phys. Rev. Lett. **98**, 175501 (2007).
[7] M. Marqués, G. J. Ackland, L. F. Lundegaard, S. Falconi, C. Hejny, M. I. McMahon, J. Contreras-García, and M. Hanfland, Origin of incommensurate modulations in the high-pressure phosphorus IV phase, Phys. Rev. B **78**, 054120 (2008).
[8] Y. Akahama, H. Kawamura, S. Carlson, T. Le Bihan, and D. H¨ausermann, Structural stability and equation of state of simple-hexagonal phosphorus to 280 GPa: Phase transition at 262 GPa, Phys. Rev. B **61**, 3139 (2000).
[9] T. Sugimoto, Y. Akahama, H. Fujihisa, Y. Ozawa, H. Fukui, N. Hirao, and Y. Ohishi, Identification of superlattice structure $cI16$ in the P-VI phase of phosphorus at 340 GPa and room temperature via x-ray diffraction, Phys. Rev. B **86**, 024109 (2012).
[10] A. S. Mikhaylushkin, S. I. Simak, B. Johansson, and U. Häussermann, High-pressure behavior of phosphorus from first principles calculations, Phys. Rev. B **76**, 092103 (2007).
[11] J. A. Flores-Livas, A. Sanna, A. P. Drozdov, L. Boeri, G. Profeta, M. Eremets, and S. Goedecker, Interplay between structure and superconductivity: Metastable phases of phosphorus under pressure, Phys. Rev. Mater. **1**, 024802 (2017).
[12] Q. Zhuang, X. Jin, K. Bao, and T. Cui, Pressure-induced metallization and reentrant insulativity in elemental crystal of phosphorus: A prediction by *ab initio* calculations, New. J. Phys. **22**, 033011 (2020).
[13] H. J. Beister, K. Strössner, and K. Syassen, Rhombohedral to simple-cubic phase transition in arsenic under pressure, Phys. Rev. B **41**, 5535 (1990).
[14] R. G. Greene, H. Luo, and A. L. Ruoff, bcc arsenic at 111 GPa: An x-ray structural study, Phys. Rev. B **51**, 597 (1995).
[15] O. Degtyareva, M. I. McMahon, and R. J. Nelmes, High-pressure structural studies of group-15 elements, High Press. Res. **24**, 319 (2004).
[16] Y. Akahama, K. Kamiue, N. Okawa, S. Kawaguchi, N. Hirao, and Y. Ohishi, V olume compression of period 4 elements: Zn, Ge, As, and Se above 200 GPa: Ordering of atomic volume by atomic number, J. Appl. Phys. **129**, 025901 (2021).
[17] O. Degtyareva, M. I. McMahon, and R. J. Nelmes, Pressure-induced incommensurate-to-incommensurate phase transition in antimony, Phys. Rev. B **70**, 184119 (2004).
[18] M. Geshi, H. Funashima, and G. P. Hettiarachchi, First-principles study of highly-compressed Sb: A stubborn body-centered cubic structure, Jpn. J. Appl. Phys. **61**, 085505 (2022).
[19] H. Luo, R. G. Greene, and A. L. Ruoff, β-Po Phase of Sulfur at 162 GPa: X-Ray Diffraction Study to 212 GPa, Phys. Rev. Lett. **71**, 2943 (1993).

[20] Y. Akahama, M. Kobayashi, and H. Kawamura, Structural studies of pressure-induced phase transitions in selenium up to 150 GPa, Phys. Rev. B **47**, 20 (1993).

[21] J. C. Jamieson and D. B. McWhan, Crystal Structure of Tellurium at High Pressure, J. Chem. Phys. **43**, 1149 (1965).

[22] G. Parthasarathy and W. B. Holzapfel, High-pressure structural phase transitions in tellurium, Phys. Rev. B **37**, 8499 (1988).

[23] J. Whaley-Baldwin, M. Hutcheon, and C. J. Pickard, Superconducting incommensurate host-guest phases in compressed elemental sulfur, Phys. Rev. B **103**, 214111 (2021).

[24] T. Sugimoto, Y. Akahama, T. Ichikawa, H. Fujihisa, N. Hirao, and Y. Ohishi, Bcc-fcc structure transition of Te, J. Phys.: Conf. Ser. **500**, 192018 (2014).

[25] Y. Akahama, N. Okawa, T. Sugimoto, H. Fujihisa, N. Hirao, and Y. Ohishi, Coexistence of a metastable double hcp phase in bcc–fcc structure transition of Te under high pressure, Jpn. J. Appl. Phys. **57**, 025601 (2018).

[26] M. Geshi and H. Funashima, First-Principles Study for High-Pressure Tellurium near a Transition from bcc to fcc, J. Phys. Soc. Jpn. **89**, 124603 (2020).

[27] P. Giannozzi, O. Andreussi, T. Brumme, O. Bunau, M. B. Nardelli, M. Calandra, R. Car, C. Cavazzoni, D. Ceresoli, M. Cococcioni, N. Colonna, I. Carnimeo, A. D. Corso, S. de Gironcoli, P. Delugas, R. A. DiStasio, A. Ferretti, A. Floris, G. Fratesi, G. Fugallo *et al.*, Advanced capabilities for materials modelling with QUANTUM ESPRESSO, J. Phys.: Condens. Matter **29**, 465901 (2017).

[28] J. P. Perdew, K. Burke, and M. Ernzerhof, Generalized Gradient Approximation Made Simple, Phys. Rev. Lett. **77**, 3865 (1996).

[29] We used the pseudopotentials P.pbe-n-rrkjus_psl.1.0.0.UPF, As.pbe-n-rrkjus_psl.1.0.0.UPF, and Sb.pbe-n-rrkjus_psl.1.0.0.UPF from http://www.quantum-espresso.org.

[30] See Supplemental Material at http://link.aps.org/supplemental/10.1103/PhysRevB.108.094112 for dependency of USPP and comparison with the FLAPW calculations.

[31] M. Geshi, H. Funashima, and G. P. Hettiarachchi, Study of compressed sulfur based on reliable first-principles calculations, Phys. Rev. B **104**, 104106 (2021).

[32] P. Blaha, K. Schwarz, G. K. H. Madsen, D. Kvasnicka, J. Luitz, R. Laskowski, F. Tran, and L. D. Marks, *WIEN2K, An Augmented Plane Wave+Local Orbitals Program for Calculating Crystal Properties* (Karlheinz Schwarz, Technische Universität Wien, Vienna, Austria, 2018).

[33] A. Togo, L. Chaput, T. Tadano, and I. Tanaka, Implementation strategies in phonopy and phono3py, J. Phys.: Condens. Matter **35**, 353001 (2023).

[34] P. Tsuppayakorn-aek, W. Luo, R. Ahuja, and T. Bovornratanaraks, The high-pressure superconducting phase of arsenic, Sci. Rep. **8**, 3026 (2018).

Understanding the difference in fragility of the bcc phases of highly compressed P, As, and Sb through first-principles investigations

Masaaki Geshi[1], Hiroki Funashima[2], Gayan Prasad Hettiarachchi[1]

[1] *R^3Institute for Newly-Emerging Science Design, Osaka University, 1-2 Machikaneyama, Toyonaka, Osaka 560-0043, Japan*

[2]*Department of Comprehensive Engineering, Kindai University Technical College, 7-1 Kasugaoka, Nabari, Mie 518-0459, Japan*

I. VALIDITY OF ULTRASOFTPSUDOPOTENTIALS

The main computational data of P was calculated using the ultrasoft pseudopotential (USPP) of P.pbe-n-rrkjus_psl.1.0.0.UPF in the pslibrary of Quantum Espresso (QE). The pseudopotential was generated with a Scalar-Relativistic Calculation and a local potential by smoothing all electron potential with Bessel functions of the cutoff radius of 1.800 bohr. The valence configuration was 5-electron $3s^2 3p^3$. Similarly, for As and Sb, As.pbe-n-rrkjus_psl.1.0.0.UPF and Sb.pbe-n-rrkjus_psl.1.0.0.UPF in the pslibrary were used for the main calculations. Those were generated with the Scalar-Relativistic Calculation, and L component and cutoff radius for local potential were 2 and 2.000 bohr for As, and with the local potential by smoothing all electron potential with Bessel functions of the cutoff radius of 2.1000 bohr for Sb. The valence configuration was 5-electron $4s^2 4p^3$ for As and 5-electron $5s^2 5p^3$ for Sb.

A. Electronic structure of hcp P

It is necessary to confirm whether these USPPs represent the correct electronic states even in calculations at ultrahigh pressures. In particular, it is important to confirm whether the states included in the core states are also treated correctly in the calculated high-pressure states. Figure 1 shows the densities of states (DOSs) of P at 1000 GPa calculated using QE with the USPP mentioned above. The cutoff energy for wavefunctions was 80 Ry and that for charge density was 960 Ry. The *k*-point sampling employed a 24 × 24 × 24 Monkhorst-Pack mesh. Figure 2 shows the DOSs calculated using the full-potential linearized augmented plane wave (FLAPW) method of WIEN2k with $R_{MT}K_{max} = 9.0$ and 490 *k*-points in an irreducible Brillouin zone. The 2*p* states lie at about -130 eV, which can be considered as the core states, and even at ultrahigh pressure of 1000 GPa, this pseudopotential is consistent with the results of the all-electron calculations.

B. Electronic structure of bcc As

Figure 3 shows the DOSs of As at 2000 GPa calculated using QE with the USPP mentioned above. The lattice constant was a = 2.1748 Å. The cutoff energy and k-point sampling conditions were similar to those used in Fig. 1. Figure 4 shows the DOS of As calculated using QE with a USPP that treats the 3d electrons as valence (15-electron $3d^{10}4s^{2}4p^{3}$). The lattice constant was a = 2.1748 Å. The calculated pressure value was 1925 GPa. Figure 5 shows the DOSs of As calculated using the FLAPW method of WIEN2k with the same lattice constant of a=2.1748 Å, $R_{MT}K_{max}$ = 9.0, and 286 k-points in an irreducible Brillouin zone. First of all, the DOSs shown in Figures 3 and 4 are consistent with each other. Moreover, the DOSs in Figures 4 and 5 are also consistent with each other. One might think that under high pressure conditions the 3d states must be treated as valence. However, the electronic states of USPP that treated the 3d electrons as core, are virtually consistent with the all-electron calculation for the most important electronic states near the Fermi level. Of course, there is an important difference between treating the 3d electrons as valence or core as mentioned below.

The orthogonality between 3d and 4d electrons is ignored when the 3d electrons are treated as core electrons. There is a possibility of the 4d states appearing near the Fermi level. In the case of the bcc structure of P in our study, the transition of the p state to the d state could destroy the bonding-antibonding state constructed by the p state, thus reducing the stability of the bcc structure. We performed the structure search using the USPP that treats 3d electrons as valence for several pressure values. From Figure 6, the transition pressure from the bcc to hcp structure shifts to higher pressure. The effects of how the 3d electrons are treated finally appears at these very high pressures. However, at lower pressures there is virtually no effect. The difference resulting from the way the 3d electrons are treated was about 75 GPa in pressure.

Figure 6 shows the total energies calculated by the USPP and FLAPW methods as a function of volume. The total energy at the volume of 69.1303 bohr^3 at 200 GPa is set to zero as the baseline. The USPP we used proves to be satisfactorily precise, consistent with the results of the FLAPW method over a wide pressure range.

C. Electronic structure of bcc Sb

Similar investigations of the electronic structure was done for bcc Sb at 1000 GPa as shown in Figures 7-9. Figure 7 shows the DOSs of Sb at 1000 GPa calculated using QE with USPP mentioned above. The lattice constant was a = 2.5995 Å. The cutoff energy and k-point sampling conditions were same as those of Figure 1. Figure 7 shows the DOSs of Sb with the lattice constant of a = 2.5995 Å calculated using QE with a USPP that

treats the 4*d* electrons as valence electrons (15-electron $4d^{10}5s^{2}5p^{3}$). The calculated pressure value is 977 GPa. Figure 8 shows the DOSs of bcc Sb calculated using the FLAPW method of WIEN2k with the same lattice constant of a = 2.5995 Å, $R_{MT}K_{max}$ = 9.0 and 286 k-points in an irreducible Brillouin zone. The DOSs in Figure 7 and those in Figure 8 are consistent with each other. Moreover, the DOSs in Figure 8 and those in Figure 9 are also consistent with each other. At least below this pressure, either USPP can be used to obtain the electronic states nearly equivalent to the FLAPW method. The difference resulting from the way the 4*d* electrons are treated was about 23 GPa in pressure.

D. Dependency of the cutoff energy on the structure search (example of As)

Although the two basic electronic states are consistent among the two USPP and FLAPW methods, the enthalpy values resulting from the total energy calculations require greater precision, since high computational precision is needed in comparing enthalpies between structures. It also affects the precision of the structural relaxation itself. In other words, calculations with low precision may converge on different structures, but calculations with high precision may converge on the same structure. We performed the structure search to cover the space groups from 75 (*P4*) to 230 ($Ia\bar{3}d$) using the USPP that treats 3*d* electrons as valence electrons. Figure 10 shows the obtained enthalpies with respect to the enthalpy of the bcc structure as a function of pressure. Each panel shows the results of different cutoff energies of (a) 60, (b) 80, and (c) 100 Ry. Because the 3*d* electrons are localized, low cutoff energy significantly affects the structure prediction, converging to the wrong structure as seen at 60 Ry. For this UPSS, the results of cutoff energies smaller than 80 Ry are not reliable. In light of this, the results of previous studies discussing the difference between the bct and bcc structures may not be accurate.

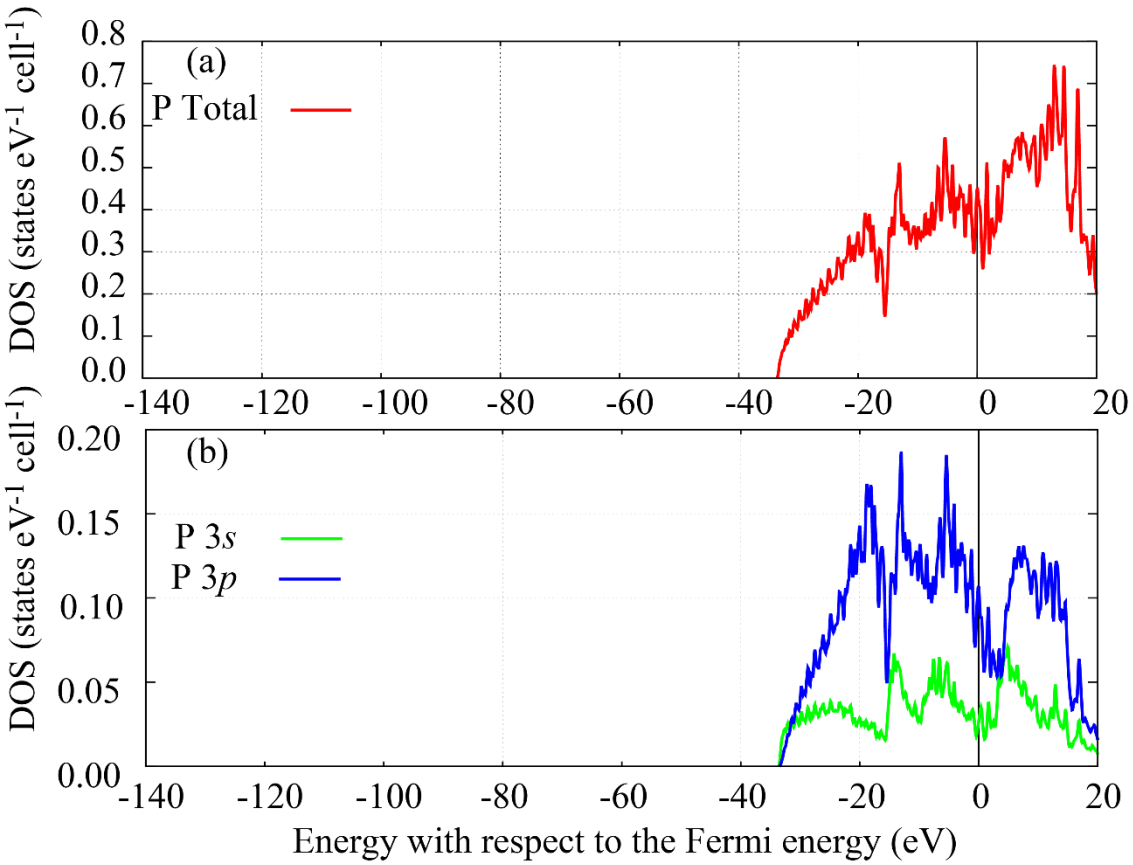

Figure. 1 (Color online)

(a) The total DOS and (b) partial DOSs of hcp P calculated using the USPP described in the text. The lattice constants are a = 1.85939 Å, c = 3.1447 Å. These are the results obtained by the structure search at 1000 GPa.

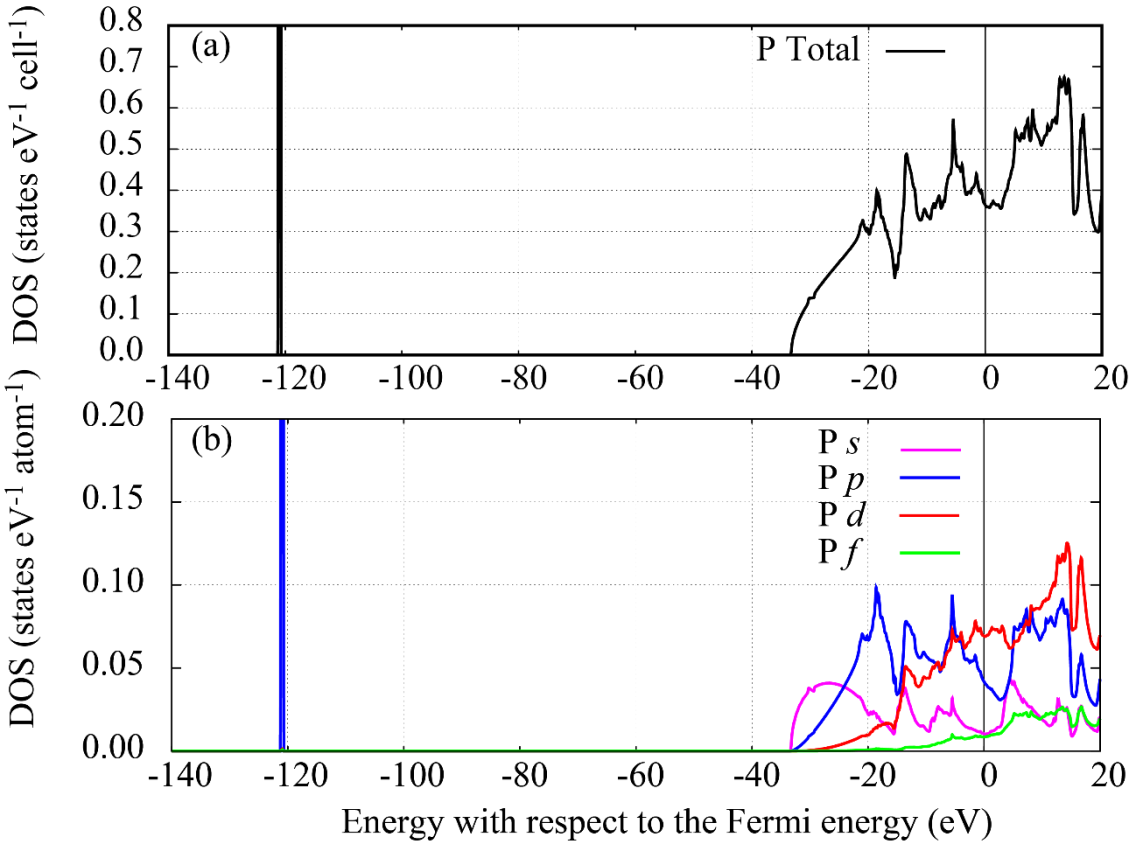

Figure. 2 (Color online)

(a) The total DOS and (b) the partial DOSs of hcp P calculated using the FLAPW method. The lattice constants are the same as in Figure 1.

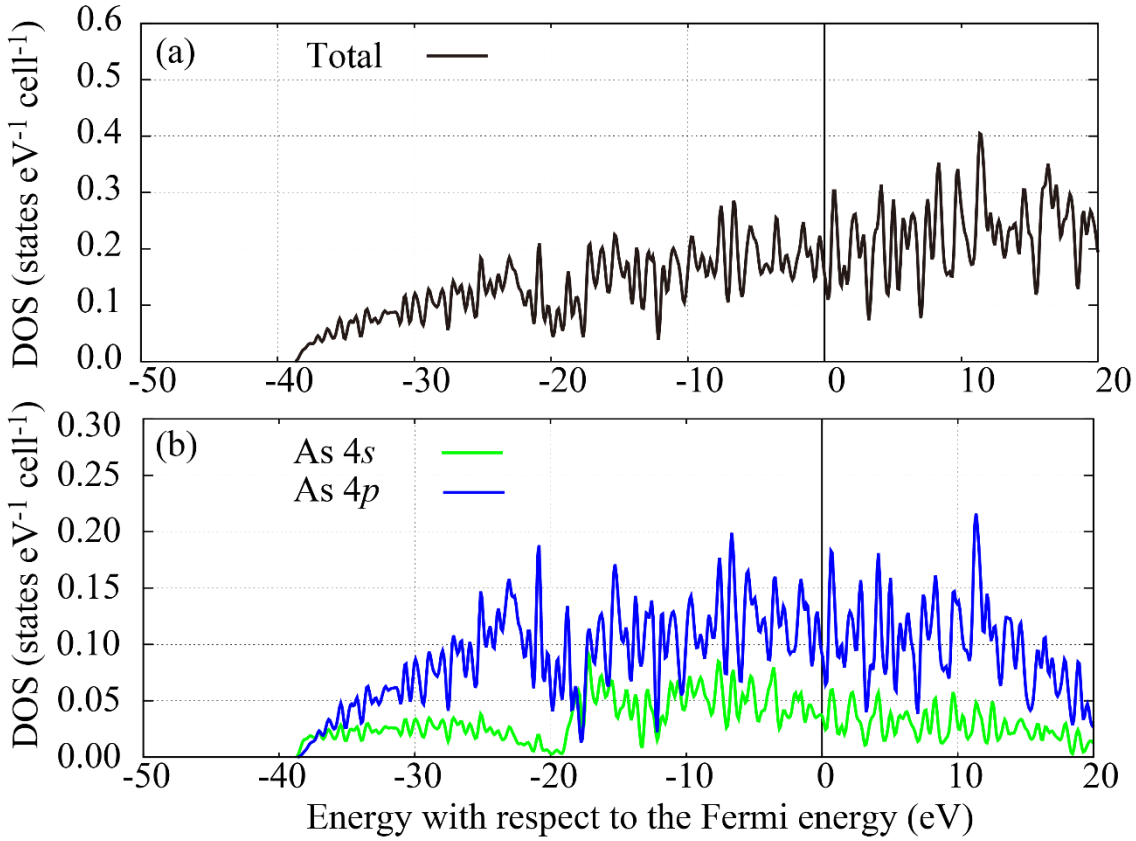

Figure. 3 (Color online)

(a) The total DOS and (b) the partial DOSs of bcc As calculated the USPP that treats the 3*d* electrons as core electrons. The lattice constant is a = 2.1748 Å. These are the results obtained by the structure search at 2000 GPa.

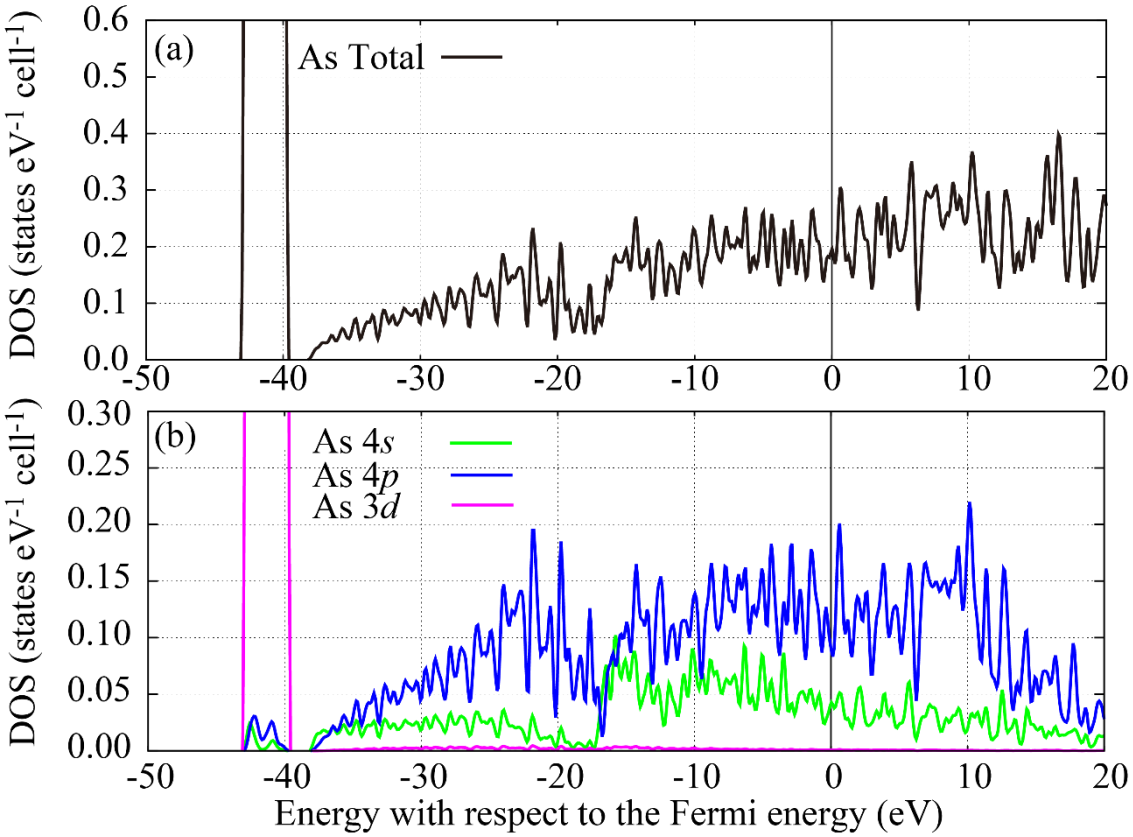

Figure. 4 (Color online)

(a) The total DOS and (b) partial DOSs of bcc As calculated with the USPP that treats the 3*d* electrons as valence electrons. The lattice constant is the same as in Figure 3, a = 2.1748 Å. The calculated pressure value in this USPP is 1925 GPa, which is slightly lower than 2000 GPa.

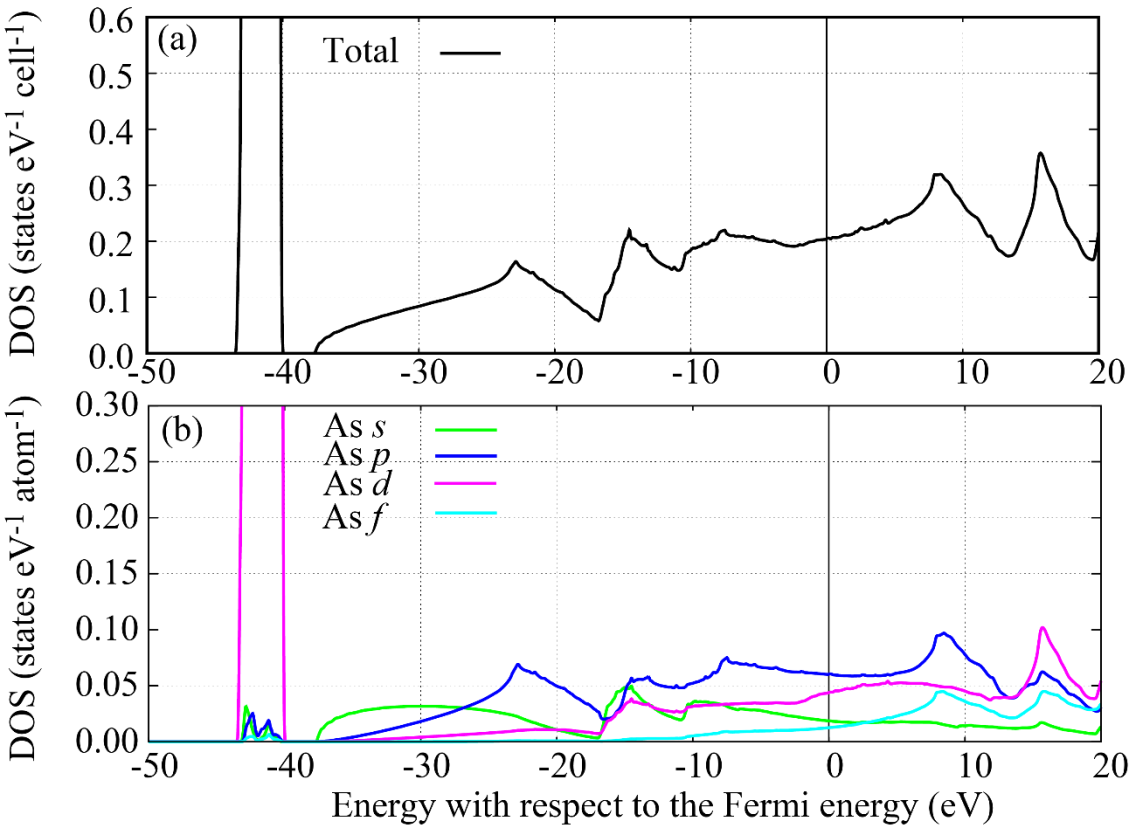

Figure. 5 (Color online)

(a) The total DOS and (b) partial DOSs of bcc As calculated using the FLAPW method with the lattice constant of a = 2.1748 Å.

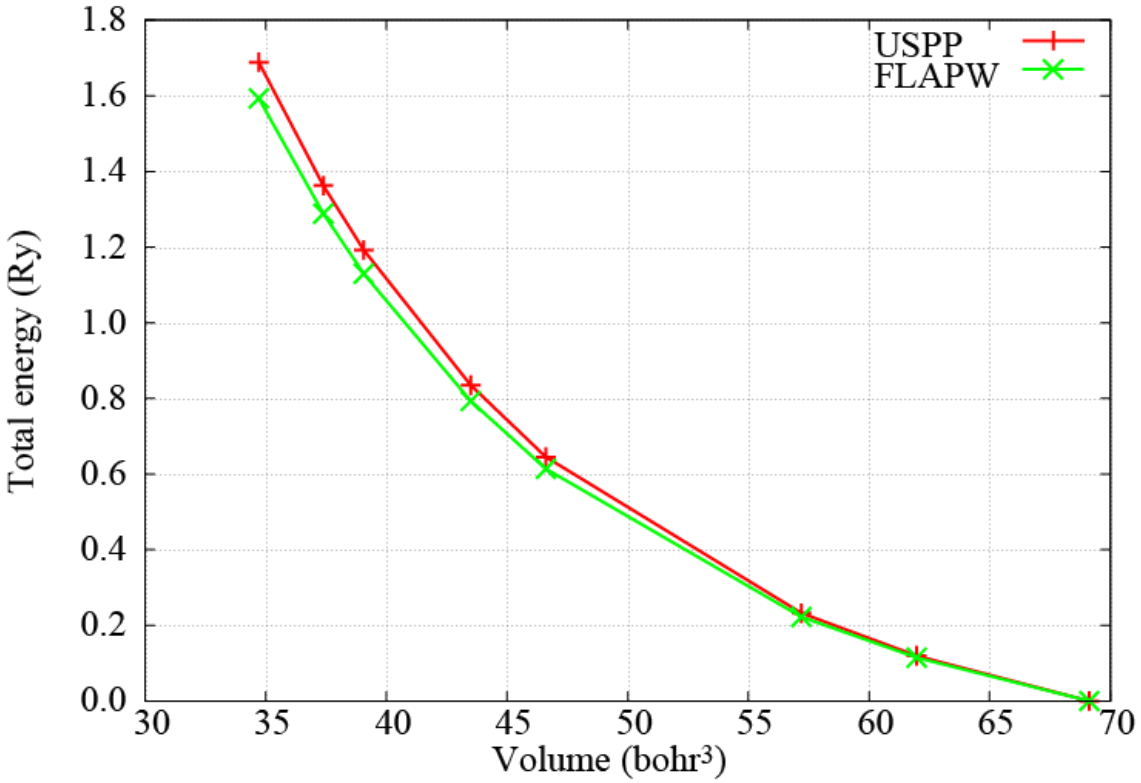

Figure. 6 (Color online)

Total energies with respect to that at 69.1303 bohr^3 as a function of volume. The volume of 69.1303 bohr^3 corresponds to the pressure of 200 GPa obtained by the calculation of QE with the USPP treating the 3*d* electrons as core electrons. These data points from right to left correspond to the pressure values of 200, 300, 400, 800, 1000, 1400, 1600, and 2000 GPa.

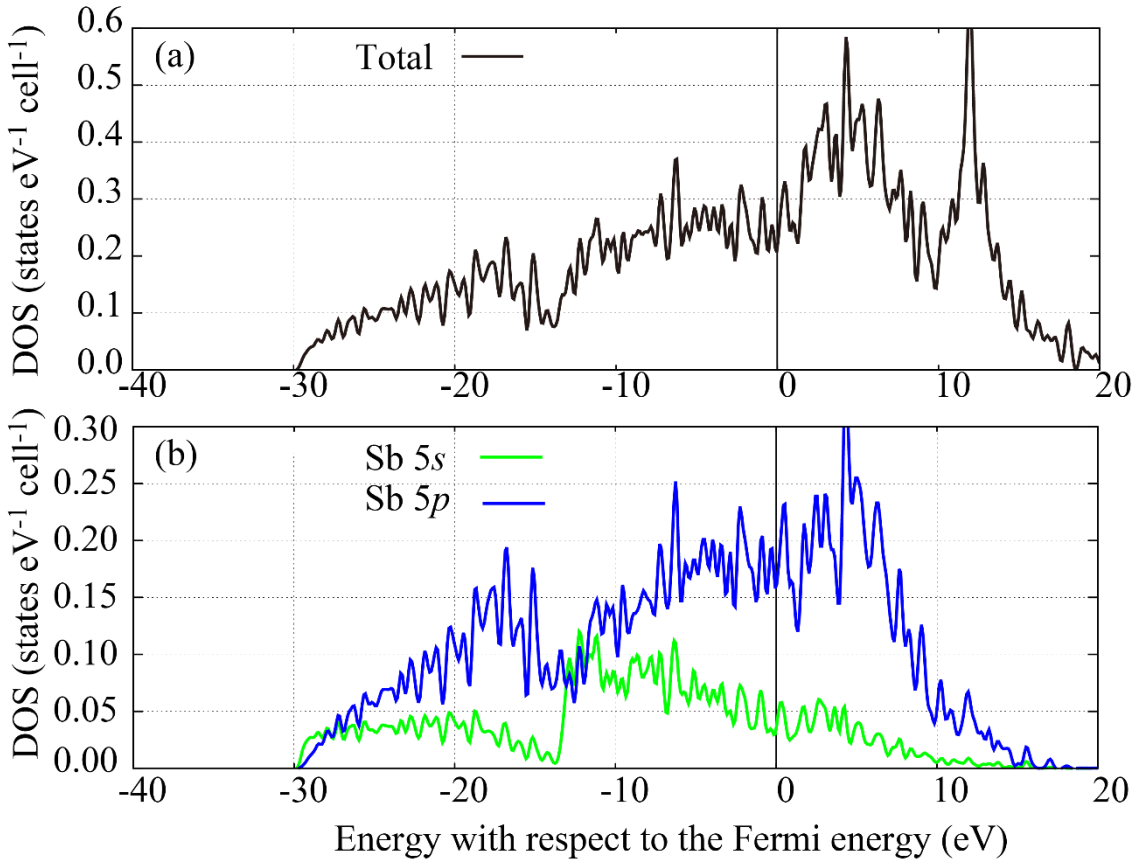

Figure. 7 (Color online)

(a) The total DOS and (b) partial DOSs of bcc Sb calculated using the USPP that treats the 4*d* electrons as core electrons. The lattice constant is $a = 2.5995$ Å, which corresponds to 1000 GPa.

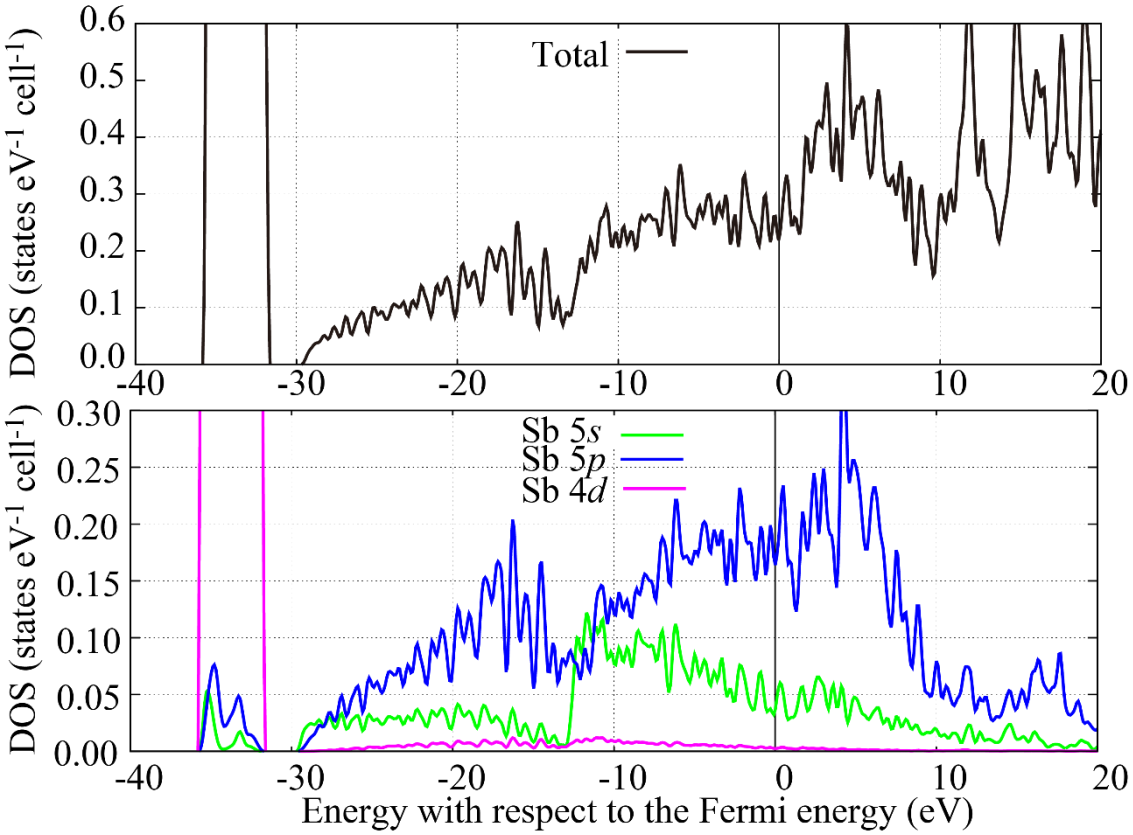

Figure. 8 (Color online)

(a) The total DOS and (b) partial DOSs of bcc Sb calculated using the USPP that treats the 4*d* electrons as valence electrons. The lattice constant is a = 2.5995 Å. The calculated pressure value in this USPP is 977 GPa, which is slightly lower than 1000 GPa.

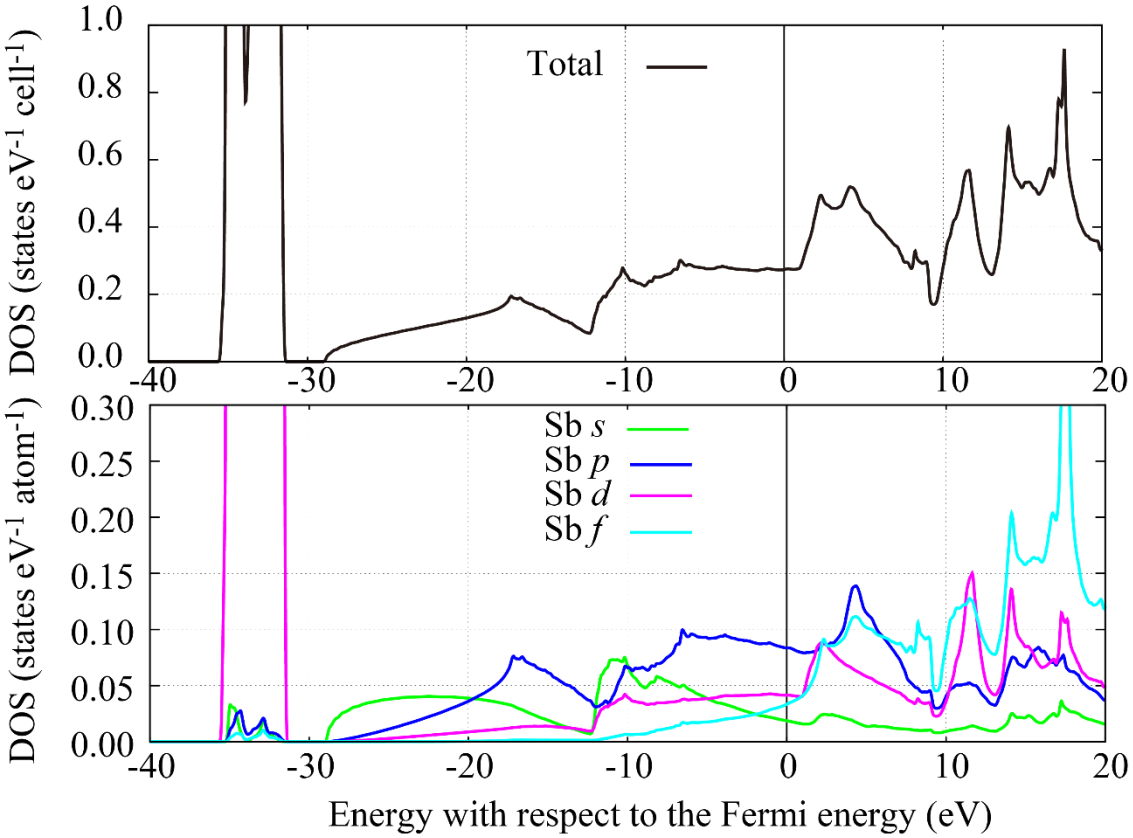

Figure. 9 (Color online)

(a) The total DOS and (b) partial DOSs of bcc Sb calculated using the FLAPW method with the lattice constant of a = 2.5995 Å.

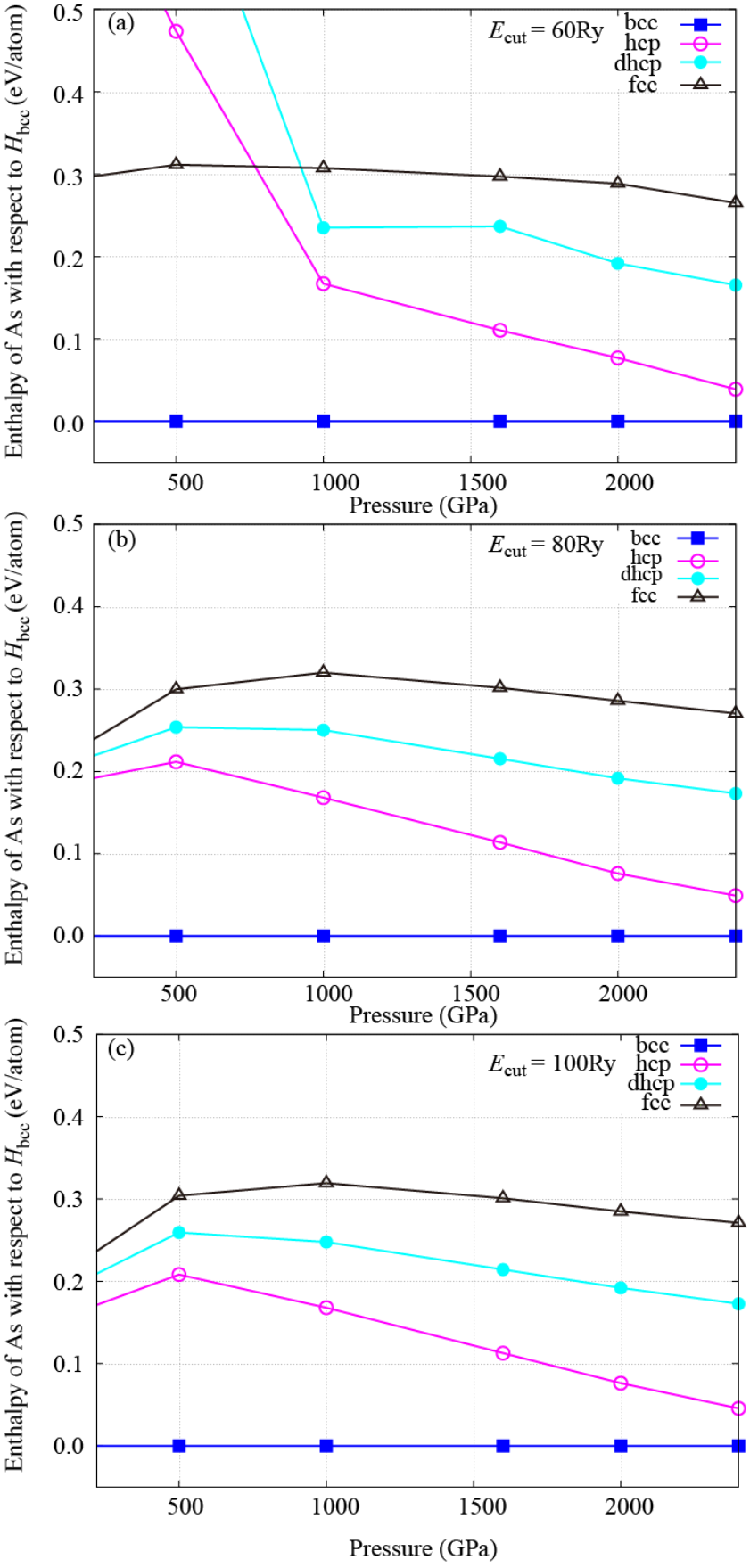
(a)
E_{cut} = 60Ry
bcc
hcp
dhcp
fcc
Enthalpy of As with respect to H_{bcc} (eV/atom)
0.5
0.4
0.3
0.2
0.1
0.0
500
1000
1500
2000
Pressure (GPa)
(b)
E_{cut} = 80Ry
bcc
hcp
dhcp
fcc
Enthalpy of As with respect to H_{bcc} (eV/atom)
0.5
0.4
0.3
0.2
0.1
0.0
500
1000
1500
2000
Pressure (GPa)
(c)
E_{cut} = 100Ry
bcc
hcp
dhcp
fcc
Enthalpy of As with respect to H_{bcc} (eV/atom)
0.5
0.4
0.3
0.2
0.1
0.0
500
1000
1500
2000
Pressure (GPa)

Figure. 10 (Color online)
The calculated enthalpies *H* of As with respect to the enthalpy of the bcc structure as a function of pressure at various cutoff energies of (a) 60 Ry, (b) 80 Ry, and (c) 100 Ry. The solid lines are guides to the eye.